Cory Thomas[1]*
Xinyu Lu[1]*
Andrew Todd[1]
Yash Raval[2]
Tzuen-Rong Tzeng[2]
Yongxin Song[3]**
Junsheng Wang[4]
Dongqing Li[5]
Xiangchun Xuan[1]

[1]Department of Mechanical Engineering, Clemson University, Clemson, SC, USA
[2]Department of Biological Sciences, Clemson University, Clemson, SC, USA
[3]College of Marine Engineering, Dalian Maritime University, Dalian, P.R. China
[4]College of Information Science and Technology, Dalian Maritime University, Dalian, P.R. China
[5]Department of Mechanical and Mechatronics Engineering, University of Waterloo, Waterloo, ON, Canada

Received June 17, 2016
Revised August 3, 2016
Accepted August 4, 2016

Research Article

Charge-based separation of particles and cells with similar sizes via the wall-induced electrical lift

The separation of particles and cells in a uniform mixture has been extensively studied as a necessity in many chemical and biomedical engineering and research fields. This work demonstrates a continuous charge-based separation of fluorescent and plain spherical polystyrene particles with comparable sizes in a ψ-shaped microchannel via the wall-induced electrical lift. The effects of both the direct current electric field in the main-branch and the electric field ratio in between the inlet branches for sheath fluid and particle mixture are investigated on this electrokinetic particle separation. A Lagrangian tracking method based theoretical model is also developed to understand the particle transport in the microchannel and simulate the parametric effects on particle separation. Moreover, the demonstrated charge-based separation is applied to a mixture of yeast cells and polystyrene particles with similar sizes. Good separation efficiency and purity are achieved for both the cells and the particles.

Keywords:
Electrical lift / Electrokinetic / Microfluidic / Particle separation / Surface charge
DOI 10.1002/elps.201600284

1 Introduction

Isolating types of particles (either synthetic or biological) from a mixture is a necessity for a wide range of chemical and biomedical applications, which has been extensively studied, particularly with microfluidic devices [1–5]. A variety of force-based *active* methods have thus far been established to separate particles in pressure-driven flows including electric [6–8], magnetic [9, 10], and acoustic [11, 12] etc. *Passive* separation methods have arisen by introducing a coordinated placement of obstacles [13, 14], fluid inertia [15, 16], or fluid elasticity [17, 18] into pressure-driven flows [19, 20]. They have also been developed in electric field driven (or simply speaking, electrokinetic) flows through the use of channel geometry (e.g., curvature or obstacles) induced particle dielectrophoresis (DEP) [21–23]. Our group has recently proposed a new kind of electrokinetic method for particle separation via the wall-induced electrical lift in a straight uniform microchannel [24]. This noninertial lift force results from the inherent electric field nonuniformity around a dielectric particle in a conducting fluid that becomes asymmetric due to the presence of a dielectric wall [25–28]. It pushes the particle away from the wall at a rate depending on its size and surface charge. The former dependence has been exploited to implement a binary and a ternary separation of polystyrene particles in a T-shaped microchannel [24]. This work is aimed to demonstrate the particle separation by surface charge via the wall-induced lateral particle migration in electrokinetic flow.

The surface charge of a particle is the electric potential difference formed spontaneously between the two surfaces at the particle–fluid interface [29]. It affects the interaction among particles and hence the stability of particle suspension [30]. It also affects the force between particles and the charged surfaces of the container for the particle suspension, and hence the particle adsorption onto these surfaces [31]. Moreover, surface charge leads to particle electrophoresis in response to electric field and determines the electrophoretic mobility [32]. The electrical feature of surface charge requires that the charge-based particle separation involves the use of electric field. Such a separation has been demonstrated in CE [33] and electrical field flow fractionation [34], both of which take place in a batch process along the axis of time.

Correspondence: Professor Xiangchun Xuan, Department of Mechanical Engineering, Clemson University, Clemson, SC 29634-0921, USA
E-mail: xcxuan@clemson.edu
Fax: +1-864-656-7299

Abbreviations: DC, direct current; **DEP**, dielectrophoresis; **PDF**, probability distribution function; **YM**, yeast mold

*Additional corresponding author: Professor Yongxin Song
E-mail: yongxin@dlmu.edu.cn.
**These authors contributed equally to this work.

Colour Online: See the article online to view Figs. 1–5 in colour.

Charge-based separation of particles has also been realized in a continuous flow along the axis of space. Free flow electrophoresis is one such method, where a transverse electric field is imposed upon a pressure-driven flow to separate particles by the charge-dependent electrophoretic migration [35]. It suffers from the issue of electrochemical reactions on the embedded electrodes [36]. In another continuous method, a bidirectional pressure and electric field driven flow in a converging–diverging microchannel can selectively trap particles bearing a specific charge at a very low throughput [37]. Recently, DEP has been utilized to direct particles against [38] or across [39] the streamlines of particle charge dependent electrokinetic transport for a continuous separation. It is the particle motion subjected to electric field gradients [40], which are induced by either the variation of channel cross-section [38] or the curvature of a microchannel [39].

In this work, we exploit the wall-induced electrical lift to separate spherical polystyrene particles with similar sizes but dissimilar charges in a ψ-shaped microchannel. We also use our previously developed theoretical model [24] to understand the particle behavior and predict the parametric effects in such a separation. Moreover, this electrokinetic separation is applied to a mixture of yeast cells and polystyrene particles with comparable sizes.

2 Experimental

2.1 Fabrication of microchannels

The microchannel shown in Fig. 1 was fabricated with PDMS using a standard soft lithography method. A complete guide for fabrication of this overall ψ-shaped channel can be referenced to Lu et al. [41]. The channel has a width of 100 μm and a depth of 25 μm throughout each branch. The three inlet branches are each 1.4 cm long, where the two outer ones are for the supply of particle mixture and the inner one (composed of multiple turns for matching the length of the outer inlet branches) is for the sheath fluid. The main branch where the particle separation takes place is 1.0 cm long. Each of the three reservoirs includes a 900 μm wide expansion in the front, where a set of five pillars are designed to control particle aggregations and PDMS debris from entering the channel at the inlets. These pillars at the exit reservoir also function as six distinct passages to visually measure particle separation. The outlet reservoir is made larger than the inlet

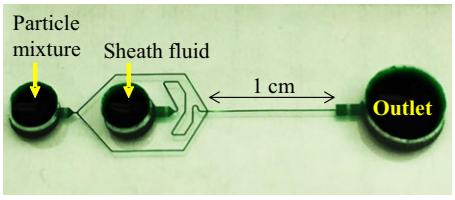

Figure 1. Top-view picture of the ψ-shaped microchannel (filled with green dye for clarity) used in experiments.

ones for the purpose of reducing the effect of backflow that is induced by the liquid buildup in electroosmosis [42].

2.2 Preparation of particle and cell solutions

The particle mixture was prepared by suspending 5 μm diameter plain polystyrene spheres (Sigma-Aldrich, St. Louis, MO) and 6 μm diameter fluorescent polystyrene spheres (Phosphorex, Hopkinton, MA) in 1 mM phosphate buffer. The final particle concentration was about 10^6 particles/mL for each type. The fluorescent particles from Phosphorex were observed to have a diameter range of 4–8 μm. Glycerol was included in the particle solution at a weight percentage of 22% in order to achieve neutral buoyancy of the particles [43]. Because of the added glycerol, adhesion effects between the channel wall and particles were also suppressed. The resulting dynamic viscosity of the particle solution was 1.908×10^{-3} kg/(m·s). The 1 mM phosphate buffer and glycerol mixture without particles was used as the sheath fluid.

For the cell separation experiment, yeast cells (*Saccharomyces cerevisiae* ATCC 9763) were procured from American Type Culture Center (Manassas, VA). They were routinely cultivated in yeast mold agar (YM agar) plates/ YM broth at 30°C. Specifically, a single colony of yeast freshly grown on YM agar plate was picked up and used for inoculating YM broth (15 mL) in a sterile tube. The cells were grown at 30°C under shaking conditions (250 rpm) for 24 h. They were then centrifuged at 5000 × *g* for 5 min. The supernatant was discarded and the cells were resuspended in 1× sterile PBS. Prior to tests, the cells were washed with PBS and centrifuged for at least three times. They were finally resuspended back in the 1 mM phosphate buffer/glycerol solution and mixed with 5 μm plain particles from Sigma. We did not use PBS to resuspend the particle and cell mixture because PBS is a highly conductive buffer and may cause significant Joule heating effects in the separation experiment [44]. We have used 1 mM phosphate buffer to resuspend yeast cells in a recent study [45] and found no apparent issues with the cell viability. The electrical conductivity of our prepared phosphate buffer/glycerol solution was measured to be around 120 μS/cm that is one order of magnitude smaller than that of PBS [46]. The final concentrations of the yeast cells and plain particles in the mixture were each adjusted to around 10^6/mL. The cells have a diameter range of 4–8 μm, which is similar to that of the fluorescent particles from Phosphorex in the particle separation experiment. Although the shapes of the yeast cells vary slightly, they are close to spheres in general.

2.3 Manipulation and visualization of particles and cells

The particles and cells in the buffer solution exhibit electrokinetic motion under direct current (DC) electric field. The DC

voltages imposed to the two inlet reservoirs (see Fig. 1) were supplied by a DC power supply (Glassman High Voltage, Inc., High Bridge) and a function generator (3322A, Agilent Technologies) in conjunction with a high-voltage amplifier (609E-6, Trek), respectively. In order to inhibit pressure-driven particle motion, the liquid levels in the three reservoirs were well balanced before every test, and each test was continuously run for no more than 3 min. The transport and separation of particles and cells were visualized and recorded using an inverted microscope (Nikon Eclipse TE2000U, Nikon Instruments) with a CCD camera (Nikon DS-Qi1Mc) at a rate of 20 frames/s. The digital videos and images were processed using the Nikon imaging software (NIS-Elements AR 3.22). Images were also postprocessed in ImageJ software (National Institute of Health) using the function "Analyze Particles." The center positions of particles or cells were used to plot the probability distribution function in Excel (Microsoft). Particle streak images were obtained by superimposing sequences of images with the maximum and minimum intensity projections for fluorescent particles and plain particles/cells, respectively. Composite particle images were obtained by stacking the superimposed images of fluorescent and plain particles through background subtraction. The electrokinetic particle/cell mobility was determined by tracking the motion of single particles or cells inside the main branch of the microchannel where DEP was absent. The measurement was conducted under a small DC electric field so that Joule heating effects were also negligible. The electrokinetic velocity of particles of cells was first calculated from the traveling distance with respect to time. It was then divided by the numerically computed local electric field in the main branch to obtain the electrokinetic mobility.

3 Theory

3.1 Mechanism of particle separation

It has been recently demonstrated [26, 27] that an off-center particle experiences an electrical lift when traveling through a straight uniform microchannel under the application of a DC electric field. This force arises from the inherent asymmetric electric field distribution about the particle due to its unmatched electric conductivity with the suspending fluid [40]. It induces a lateral migration of the particle away from the channel wall toward the center [43], U_w, which, at the leading order for a remote sphere, is given by [47]:

$$\mathbf{U}_w = \frac{\varepsilon a \mathbf{E}^2}{32\eta}\left(\frac{a}{h}\right)^4 \mathbf{n}, \tag{1}$$

where ε is the fluid permittivity, a the particle radius, $\boldsymbol{E}$ the applied DC electric field in the absence of the particle, η the fluid dynamic viscosity, h the distance of the particle center from the wall, and $\boldsymbol{n}$ the unit vector normal to the wall. This transverse particle motion competes with the axial electrokinetic motion, $\boldsymbol{U}_{EK}$,

$$\mathbf{U}_{EK} = \frac{\varepsilon\left(\zeta_p - \zeta_w\right)}{\eta}\mathbf{E} = \mu_{EK}\mathbf{E}, \tag{2}$$

where ζ_p is the particle zeta potential, ζ_w the wall zeta potential, and μ_{EK} the particle's electrokinetic mobility. The rate of the resulting cross-stream deflection is determined by the transverse to axial particle velocity ratio, i.e.,

$$\frac{U_w}{U_{EK}} = \frac{a}{32}\left(\frac{a}{h}\right)^4 \frac{E}{\zeta_p - \zeta_w}, \tag{3}$$

which is a function of particle size (a) and surface charge (ζ_p). The latter dependence enables the separation of particles by charge if a sheath fluid is used to prefocus the particle mixture to a narrow stream near either sidewall a microchannel (see Fig. 1). It is important to note this charge-based particle separation is unavailable for the electrical pinched flow fractionation that, as demonstrated by Kawamata et al. [48], is capable of separating particles by size only.

3.2 Numerical simulation

The Lagrangian tracking method based theoretical model that was developed in our earlier work [24] was employed to simulate the particle trajectory in MATLAB (MathWorks). The following assumptions were made in this model: (i) only single particles are considered and the particle–particle interactions are neglected; (ii) the rotation of a particle has an insignificant effect on its translation; (iii) the inertial effect is negligible due to the small Reynolds number ($\mathrm{Re} < 0.1$); (iv) fluid properties remain unvaried because the Joule heating induced temperature rise, $\Delta T = \sigma E^2 l^2/k$ [49], is negligible, where $\sigma = 120$ μS/cm is the measured electric conductivity of the suspending fluid, $k = 0.6$ W/(m·K) the thermal conductivity of the fluid (assumed equal to that of water), and $l = 40$ μm the hydraulic diameter of the microchannel. The instantaneous position of particle center, $\boldsymbol{x}_p$, was obtained by integrating the particle velocity $\boldsymbol{U}_p$, over time, t,

$$\mathbf{x}_p = \mathbf{x}_0 + \int_0^t \mathbf{U}_p(\tau)d\tau \tag{4}$$

$$\mathbf{U}_p = \mathbf{U}_{EK} + \mathbf{U}_{DEP} + \mathbf{U}_w, \tag{5}$$

where $\boldsymbol{x}_0$ is the initial particle position and $\boldsymbol{U}_{DEP}$ is the velocity of particle DEP given by:

$$\mathbf{U}_{DEP} = -\frac{\varepsilon a^2}{3\eta}\left(\mathbf{E}\cdot\nabla\right)\mathbf{E} \tag{6}$$

It is important to note that $\mathbf{U}_{DEP}$ occurs only in the regions where inherent electric field gradients are created by the variation in channel geometry in the absence of particles (e.g., channel turns [50]). In contrast, $\mathbf{U}_w$ exists even in a straight microchannel with a uniform distribution of electric field. Such a treatment in Eq. (5) has been validated in our recent work [24]. In obtaining Eq. (6), the so-called Clausius–Mossotti factor [51] was assumed to be −0.5 considering

the much lower electric conductivity of particles than that of the suspending fluid. The electric field was solved from Laplace's equation using a 2D model in COMSOL (COMSOL Inc.), where the computational domain is identical to the microchannel in Fig. 1. The two inlet reservoirs (more accurately, the electrodes at the centers of the reservoirs) were each applied with an electric potential whereas the outlet reservoir was grounded. Insulated boundary condition was applied to other boundaries. The electrokinetic mobility, μ_{EK}, was to be 1.2×10^{-8} $m^2/(V \cdot s)$ for plain particles from Sigma and 0.3×10^{-8} $m^2/(V \cdot s)$ for fluorescent particles from Phosphorex, respectively. The majority of the yeast cells were observed to have a similar electrokinetic mobility to the fluorescent particles.

4 Results and discussion

4.1 Charge-based separation of plain and fluorescent particles

Figure 2 shows the charge-based separation of 5 μm plain and 6(± 2) μm fluorescent particles via the wall-induced electrical lift. The inlet reservoirs for particle mixture and sheath fluid (see Fig. 1) are imposed with 300 and 600 V DC, respectively, whereas the outlet reservoir is grounded. Our model in COMSOL indicates that the resulting electric field is about 15 and 252 V/cm in the inlet branch for particle mixture and sheath fluid, respectively. The electric field in the main branch is about 267 V/cm due to the mass continuity and the uniform fluid and channel properties [52]. The stream width ratio between the sheath fluid and particle mixture in the main branch is equal to the electric field ratio in between the corresponding inlet-branches, which is approximately 17:1. Therefore, each particle stream becomes $100/(17+1+1) = 5.3$ μm wide on entering into the main branch, wherein both types of particles align along the sidewall (see Fig. 2, left panel). These prefocused particles are then deflected away by the wall-induced electrical lift force when moving through the main branch. Due to the surface charge dependent deflection rate in Eq. (3), the fluorescent particles (appearing white) exhibit a larger deflection than that of the plain particles (appearing black) as illustrated in Fig. 2 (middle panel). The result is three continuously separated particle streams at the expansion of the main branch, where the two outer streams are for plain particles and the inner one is for fluorescent particles. These particle focusing, deflection, and separation processes are all simulated by our numerical model in Fig. 2 (bottom row) with a good agreement.

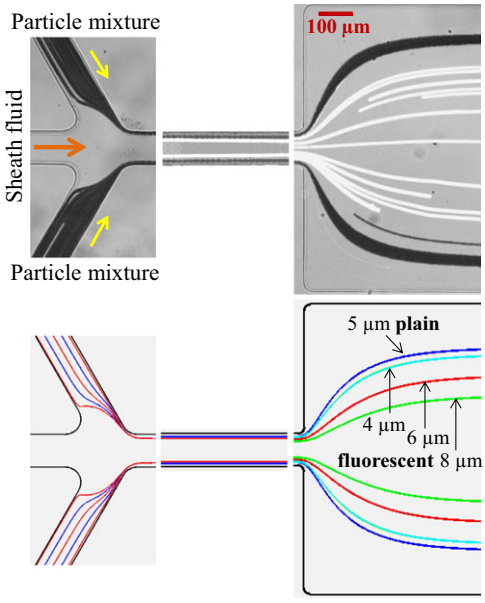

Figure 2. Demonstration of charge-based separation of 5 μm plain and 6(± 2) μm fluorescent spherical particles via the wall-induced electrical lift: experimentally obtained composite images (top row, white for fluorescent particles and black for plain ones) and numerically predicted trajectories (bottom row, red lines for fluorescent particles and blue lines for plain ones) at the trifurcation (left), the middle of the main branch (middle), and the expansion of the main branch (right). The numerically predicted trajectories of 4 and 8 μm fluorescent particles are also included in the simulation plot at the expansion of the main branch (right panel on the bottom) to account for the influence of particle size on separation. The inlet reservoirs for particle mixture and sheath fluid are imposed with 300 and 600 V DC, respectively, and the outlet reservoir is grounded.

It is, however, noted from the experimental image in Fig. 2 that the plain particle streams remain narrow while the fluorescent particle stream is significantly widened at the expansion of the main branch (top-right panel). This is attributed to the intrinsic size deviation of the latter particles from Phosphorex. To account for this influence, we have also simulated the trajectories of fluorescent particles with the diameters of 4 and 8 μm, which are included in the simulation plot (bottom-right panel). It is shown that the span of the fluorescent particles of various sizes in the simulation agree well with the experimental image. Moreover, the 4 μm fluorescent particle still has a larger deflection than the 5 μm plain one due to the former's lower electrokinetic mobility. Therefore, the separation demonstrated in Fig. 2 is primarily based on the difference in particle charge, where the size difference has only a minor effect.

4.1.1 Effect of electric field ratio

Figure 3 shows the effect of the electric field ratio in between the inlet branches for sheath fluid and particle mixture on the particle separation by charge. This is studied by fixing the voltage at the inlet reservoir for particle mixture, $\phi_{particle}$, at 300 V DC while varying that for the sheath fluid, ϕ_{sheath}, from 400 to 650 V DC. The calculated values of the electric field ratio and the prefocused particle stream width at the trifurcation are displayed in Table 1. Due to symmetry, only half of the microchannel is shown in Fig. 3 for both experiment and simulation to save space. It is shown that the numerical results of the particle trajectories agree reasonably with the

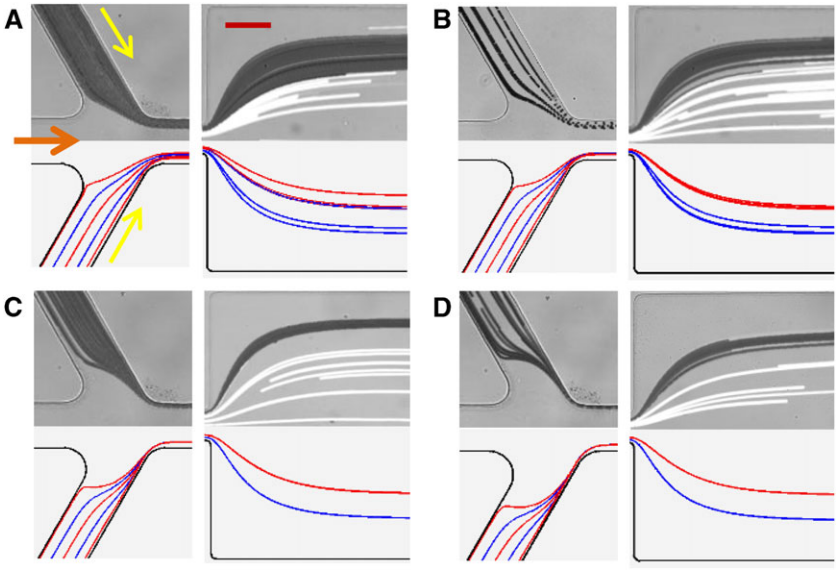

Figure 3. Experimental (top half, composite images) and numerical (bottom half) results for the effect of electric field ratio in between the inlet branches for sheath fluid and particle mixture on the charge-based separation of 5 μm plain and 6 μm fluorescent particles: at the trifurcation (left) and the expansion of the main branch (right). The DC voltage at the inlet reservoir for sheath fluid is varied from 400 V (A) to 500 V (B), 600 V (C), and 650 V (D) while that for the particle mixture is fixed at 300 V. Other conditions are referred to the caption of Fig. 2. The block arrows indicate the particle and fluid flow directions. The scale bar represents 100 μm.

Table 1. Calculated electric field ratio in between the inlet branches for sheath fluid and particle mixture and particle stream width at the trifurcation

$\phi_{particle}$ (V)	ϕ_{sheath} (V)	Ratio of electric field	Particle stream width (μm)
300	400	2.7	22.2
300	500	5.9	13.4
300	600	17	5.3
300	650	46	4.0[a)]

$\phi_{particle}$ and ϕ_{sheath} represent the DC voltages imposed to the inlet reservoirs for particle mixture and sheath fluid (see Fig. 1), respectively.
a) This value is equal to the diameter of the smallest fluorescent particles in the separation because the calculated value of 2.1 μm does not account for the contribution of particle size.

experimental observations. At $\phi_{sheath} = 400$ V, particles are weakly focused at the trifurcation because the particle stream width is much larger than the particle diameter. Therefore, the two types of particles still overlap at the expansion of the main branch, leading to an incomplete separation as viewed from Fig. 3A. With the increase of ϕ_{sheath} to 500 V and hence the electric field ratio, the particle focusing becomes better at the trifurcation and hence the two particle streams are separated apart at the expansion in Fig. 3B. This separation is further enhanced at a higher value of ϕ_{sheath} due to both the improved particle focusing at the trifurcation and the increased particle deflection in the main branch (see Fig. 3C and D). Meanwhile, however, the increase in ϕ_{sheath} also results in a quickly decreased particle throughput. Therefore, a moderate value of ϕ_{sheath} or electric field ratio, at which the particles to be separated can be aligned with a stream width of no more than two particle diameters, is appropriate for an effective separation when considering the particle throughput.

4.1.2 Effect of electric field magnitude

Figure 4 shows the experimental and numerical results of electric field magnitude effect on the charge-based separation at the outlet expansion. The inlet reservoir for sheath fluid is subjected to a range of DC voltages from 200 to 800 V whereas the voltage ratio (and hence the electric field ratio) between the sheath fluid and particle mixture is maintained at 2 (or accordingly a fixed electric field ratio of 17; see Table 1). The corresponding electric field magnitude in the main branch is increased from 89 to 179, 267, 358 V/cm in order. Due to the constant electric field ratio, the width of the focused particle stream at the trifurcation remains unvaried for all the tested voltages. However, the electrical lift induced deflection increases with increasing electric field for each type of particles [see Eq. (3)], leading to an enhanced separation between them. This trend is clear in Fig. 4 when the DC voltage for sheath fluid increases from 200 to 600 V. At 200 V, the particle throughput is the lowest due to the slowest electrokinetic flow, and hence the particle number in the superimposed image in Fig. 4A is small. With an increased voltage, more particles are able to be sorted in the same period of time, and the separation also becomes better in Fig. 4B for 400 V and Fig. 4C for 600 V, respectively. However, when the voltage for sheath fluid is further increased to 800 V in Fig. 4D, the experimental result appears to show a worse separation. This is probably due to the particle–particle interactions that become much stronger at higher electric fields. For example, the arrow in Fig. 4D highlights the trajectory of a plain particle attached to a fluorescent particle that moves inside the fluorescent particle band. Both particle bands are less focused as compared with the 600 V case though their deflections still increase. Therefore, a higher voltage does not necessarily lead to a better separation. Since the particle–particle interaction is not considered in the model, the numerical prediction at 800 V still predicts a distinct separation.

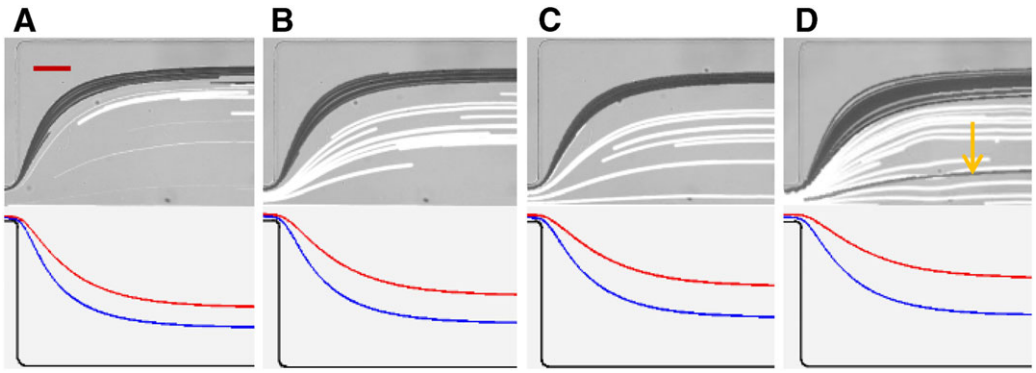

Figure 4. Experimental (top half, composite images) and numerical (bottom half) results of electric field magnitude effect on the charge-based separation of 5 μm plain and 6 μm fluorescent particles at the expansion of the main branch. The DC voltage at the inlet reservoir for sheath fluid is subjected to 200 V (A), 400 V (B), 600 V (C), and 800 V (D), respectively, while the voltage ratio between sheath fluid and particle mixture is maintained at 2. The arrow in (D) highlights the trajectory of a plain particle attached to a fluorescent one. The scale bar represents 100 μm.

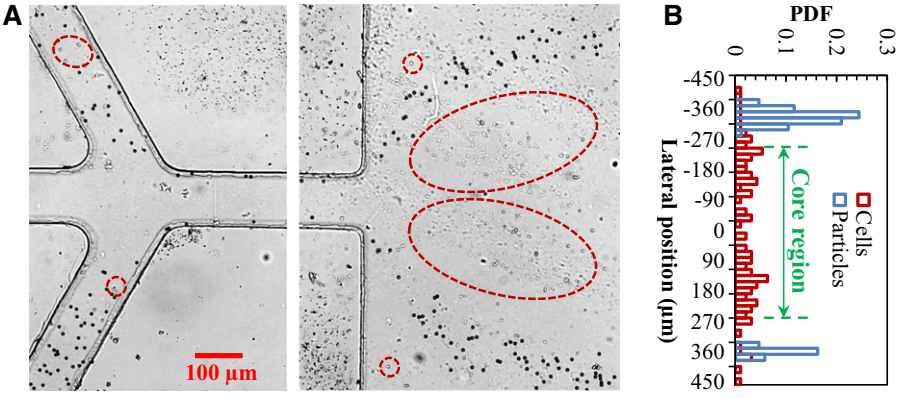

Figure 5. Charge-based separation of yeast cells (highlighted by the circles) and 5 μm plain particles via the wall-induced electrical lift. (A) Experimental image at the trifurcation (left) and the expansion of the main branch (right); (B) the probability distribution function plot of cells and particles obtained from the image sequence taken at the expansion of the main branch. The core region that was used in evaluating the cell and particle separation efficiency and purity is highlighted on the plot.

4.2 Charge-based separation of particles and cells

Figure 5 demonstrates a charge-based separation of yeast cells from 5 μm plain particles via the wall-induced electrical lift. The cells are highlighted by the circles on the images. The DC voltages at the inlet reservoirs for sheath fluid and particle mixture are 400 and 200 V, respectively. The electric field is 10 and 169 V/cm in the inlet branch for particle mixture and sheath fluid, respectively. The electric field in the main branch, which is 179 V/cm, is thus moderate and has no apparent adverse impact on cells [46]. Referring to Table 1, the particles and cells in the mixture are both well focused at the trifurcation as seen from Fig. 5A (left). As they have a comparable size distribution and electrokinetic mobility to the 6 μm fluorescent particles, yeast cells experience a greater deflection than 5 μm plain particles in the main branch. Analogous to the results in Figs. 2–4, a good separation is obtained for yeast cells from 5 μm plain particles as demonstrated in Fig. 5A (right). The distributions of probability distribution function for the cells and particles in this separation are plotted in Fig. 5B, where more than 100 cells and 200 particles were analyzed. It is found that the separation efficiency for yeast cells, which is defined as the cell percentage inside the core region with an off-center distance of 270 μm (see the highlighted region in Fig. 5B), is 83%. In contrast, the separation efficiency for plain particles outside the core region can reach 100%. The separation purity for yeast cells, i.e. the ratio of the targeted to the total collected cells inside the core region, is 100%, while that for plain particles is 94.1% outside the core region.

5 Concluding remarks

We have demonstrated a continuous charge-based separation of spherical fluorescent and plain particles with similar sizes in a ψ-shaped microchannel via the wall-induced electrical lift. The particles in the suspension are first prefocused by an electroosmotic sheath flow to a tight stream near either sidewall of the main branch. They are subsequently deflected away from the channel wall at a surface charge dependent rate. The focusing of particles and its effect on particle separation are studied by varying the electric field ratio in between the inlet branches for sheath fluid and particle mixture. The deflection of particles and its effect on particle separation are studied by varying the electric field magnitude in the main branch. The particle transport in the microchannel and the parametric effects on particle separation are all reasonably

simulated by a Lagrangian tracking method based theoretical model. We have also applied the demonstrated charge-based separation method to a mixture of yeast cells and polystyrene particles with comparable sizes. A separation efficiency of over 80% can be achieved for yeast cells with a purity of 100%.

This work is supported in part by NSF under grant CBET-1150670 and by Clemson University through the Honors and Creative Inquiry programs (X. Xuan). The support from University 111 Project of China under Grant B08046 is also gratefully acknowledged (Y. Song).

The authors have declared no conflict of interest.

6 References

[1] Pamme, N., *Lab Chip* 2007, *7*, 1644–1659.

[2] Lenshof, A., Laurell, T., *Chem. Soc. Rev.* 2010, *39*, 1203–1217.

[3] Karimi, A., Yazdi, S., Ardekani, A. M., *Biomicrofluid.* 2013, *7*, 021501.

[4] Sajeesh, P., Sen, A. K., *Microfluid. Nanofluid.* 2014, *17*, 1–52.

[5] Shields, C. W., IV, Reyes, C. D., López, G. P., *Lab Chip* 2015, *15*, 1230–1249.

[6] Kang, Y., Li, D., *Microfluid. Nanofluid.* 2009, *6*, 431–460.

[7] Pethig, R., *Biomicrofluidics* 2010, *4*, 022811.

[8] Cetin, B., Li, D., *Electrophoresis* 2011, *32*, 2420–2427.

[9] Pamme, N., *Lab Chip* 2006, *6*, 24–38.

[10] Gijs, M. A. M., Lacharme, F., Lehmann, U., *Chem. Rev.* 2010, *110*, 1518–1563.

[11] Laurell, T., Peterson, F., Nilsson, A., *Chem. Soc. Rev.* 2007, *36*, 492–506.

[12] Lin, S. S., Mao, X., Huang, T., *Lab Chip* 2012, *12*, 2766–2770.

[13] Huang, L., Cox, E. C., Austin, R. H., Sturm, J. C., *Science* 2004, *304*, 987–990.

[14] Choi, S., Song, S., Choi, C., Park, J. K., *Anal. Chem.* 2009, *81*, 1964–1968.

[15] Amini, H., Lee, W., Di Carlo, D., *Lab Chip* 2014, *14*, 2739–2761.

[16] Zhang, J., Yan, S., Yuan, D., Alici, G., Nguyen, N. T., Warkiani, M. E., Li, W., *Lab Chip* 2016, *16*, 10–34.

[17] Liu, C., Xue, C., Chen, X., Shan, L., Tian, Y., Hu, G., *Anal. Chem.* 2015, *87*, 6041–6048.

[18] Lu, X., Zhu, L., Hua, R., Xuan, X., *Appl. Phys. Lett.* 2015, *107*, 264102.

[19] Bhagat, A. A. S., Bow, H., Hou, H., Tan, S., Han, J., Lim, C., *Med. Biol. Eng. Comput.* 2010, *48*, 999–1014.

[20] Martel, J. M., Toner, M., *Annu. Rev. Biomed. Eng.* 2014, *16*, 371–396.

[21] Srivastava, S. K., Gencoglu, A., Minerick, A. R., *Anal. Bioanal. Chem.* 2010, *399*, 301–321.

[22] Regtmeier, J., Eichhorn, R., Viefhues, M., Bogunovic, L., Anselmetti, D., *Electrophoresis* 2011, *32*, 2253–2273.

[23] Li, M., Li, W., Zhang, J., Alici, G., Wen, W., *J. Phys. D Appl. Phys.* 2014, *47*, 063001.

[24] Lu, X., Hsu, J. P., Xuan, X., *Langmuir* 2015, *31*, 620–627.

[25] Young, E. W., Li, D., *Langmuir* 2005, *21*, 12037–12046.

[26] Liang, L., Ai, Y., Zhu, J., Qian, S., Xuan, X., *J. Colloid Interface Sci.* 2010, *347*, 142–146.

[27] Kazoe, Y., Yoda, M., *Langmuir* 2011, *27*, 11481–11488.

[28] Liang, Q., Zhao, C., Yang, C., *Electrophoresis* 2015, *36*, 731–736.

[29] Hunter, R. J., *Zeta Potential in Colloid Science*, Academic Press, New York 1981.

[30] Russel, W. B., Saville, D. A., Schowalter, W. R., *Colloidal Dispersions*, Cambridge University Press, Cambridge, UK 1992.

[31] Kirby, B., *Micro- and Nanoscale Fluid Mechanics: Transport in Microfluidic Devices*, Cambridge University Press, New York, USA 2010.

[32] Lyklemma, J., *Fundamentals of Interface and Colloid Science*, Academic Press, Cambridge, UK 1991.

[33] Rodriguez, M. A., Armstrong, D. W., *J. Chromatogr. B* 2004, *800*, 7–25.

[34] Giddings, J. C., *Science* 1993, *206*, 1456–1465.

[35] Kova, L., Bocek, P., *Electrophoresis* 1998, *19*, 1064–1074.

[36] Kohlheyer, D., Eijkel, J. C. T., van den Berg, A., Schasfoort, R. B. M., *Electrophoresis* 2008, *29*, 977–993.

[37] Jellema, L. C., Mey, T., Koster, S., Verpoorte, E., *Lab Chip* 2009, *9*, 1914–1925.

[38] Patel, S., Qian, S., Xuan, X., *Electrophoresis* 2013, *34*, 961–968.

[39] Zhu, J., Xuan, X., *Biomicrofluid.* 2011, *5*, 024111.

[40] Pohl, H. A., *Dielectrophoresis*, Cambridge University Press, Cambridge 1978.

[41] Lu, X., Patel, S., Zhang, M., Joo, S. W., Qian, S., Ogale, A., Xuan, X., *Biomicrofluidics* 2014, *8*, 021802.

[42] Yan, D., Yang, C., Huang, X., *Microfluid. Nanofluid.* 2007, *3*, 333–340.

[43] Liang, L., Qian, S., Xuan, X., *J. Colloid Interface Sci.* 2010, *350*, 377–379.

[44] Xuan, X., *Electrophoresis* 2008, *29*, 33–43.

[45] Patel, S., Showers, D., Vedantam, P., Tzeng, T., Qian, S., Xuan, X., *Biomicrofluidics* 2012, *6*, 034102.

[46] Voldman, J., *Annu. Rev. Biomed. Eng.* 2006, *8*, 425–454.

[47] Yariv, E., *Phys. Fluids* 2006, *18*, 031702.

[48] Kawamata, T., Yamada, M., Yasuda, M., Seki, M., *Electrophoresis* 2008, *29*, 1423–1430.

[49] Ramos, A., Morgan, H., Green, N. G., Castellanos, A., *J. Phys. D Appl. Phys.* 1998, *31*, 2338–2353.

[50] Zhu, J., Tzeng, T. R., Xuan, X., *Electrophoresis* 2010, *31*, 1382–1388.

[51] Chang, H. C., Yeo, L. Y., *Electrokinetically-Driven Microfluidics and Nanofluidics*, Cambridge University Press, Cambridge, UK 2009.

[52] Xuan, X., Li, D., *Electrophoresis* 2005, *26*, 3552–3560.

